Neutrino magnetic moment and inert doublet dark matter in a Type-III radiative scenario

Shivaramakrishna Singirala,[*] Dinesh Kumar Singha,[†] and Rukmani Mohanta[‡]
School of Physics, University of Hyderabad, Hyderabad 500046, India

(Received 6 July 2023; accepted 28 October 2023; published 29 November 2023)

We examine dark matter, neutrino magnetic moment, and mass in a Type-III radiative scenario. The Standard Model is enriched with three vectorlike fermion triplets and two inert doublets to provide a suitable platform for the above phenomenological aspects. The inert scalars contribute to the total relic density of dark matter in the Universe. Neutrino aspects are realized at one loop with the magnetic moment obtained through charged scalars, while the neutrino mass gets contributions from charged and neutral scalars. Taking inert scalars up to 2 TeV and triplet fermions in the few hundred TeV range, we obtain a common parameter space, compatible with experimental limits associated with both neutrino and dark matter sectors. Using a specific region for the transition magnetic moment [$\mathcal{O}(10^{-11}\mu_B)$], we explain the excess recoil events, reported by the XENON1T Collaboration. Finally, we demonstrate that the model is able to provide neutrino magnetic moments in a wide range from $10^{-12}\mu_B$ to $10^{-10}\mu_B$, meeting the bounds of various experiments such as Super-K, TEXONO, Borexino, and XENONnT.

DOI: 10.1103/PhysRevD.108.095048

I. INTRODUCTION

The fascinating description of elementary particle physics is elegantly portrayed by the Standard Model (SM) in the low-energy regime. The locally gauge-invariant Lagrangian is able to describe how the interactions proceed at the most fundamental level. This gauge theory has provided a pathway to understand the behavior of nature at a very tiny length scale and serves as a theoretical torch for exploring several unknown things beyond, a never-ending tale of theorists and experimentalists to unravel the mysteries of the Universe. A small chunk of puzzles include neutrino masses and mixing [1–10], the nature and identity of dark matter (DM) [11–14], matter-antimatter asymmetry [15–18], and the recently observed anomalies in the flavor sector [19].

Several neutrino experiments have unambiguously proved that oscillation of neutrino flavor occurs during propagation, and that neutrinos possess small but nonzero masses. With this extra degree of freedom, many new possibilities are opened up, and one such possibility among them is that neutrinos can possess electromagnetic properties like electric and magnetic dipole moments. Solar, accelerator, and reactor experiments help us in the direct measurement of magnetic moments and eventually put limits on them. One possible mode of measurement involves the study of neutrino/antineutrino electron scattering at low-energy limits. In minimally extended SM, one can have a neutrino magnetic moment (νMM) of the order 10^{-19} μ_B for Dirac-type neutrinos. However, these values are beyond the sensitivity reach of any experimental measurement. On the other hand, for Majorana-type neutrinos, one can have a very high transition magnetic moment, fitting the experimental observations. That is why the study of νMM becomes important for the distinction of Dirac and Majorana types of neutrinos.

In the recent past, the XENON Collaboration performed a search for new physics with its 1 ton detector and reported an excess of events over the known backgrounds in the recoil energy range 1–7 keV, peaked around 2.5 keV [20]. It turns out that such excess can be explained with a large transition magnetic moment of neutrinos. With new data from its successor XENONnT [21], no visibly bold excess events were seen in the low-energy region, creating an anomalous situation between these two experiments. The collaboration is suspecting this excess in XENON1T was due to uncounted tritium, whose presence or absence they cannot corroborate. In this scenario, we cannot completely ignore the possible implication of new physics effects at XENON1T, and that is why it is very interesting to explore such possibilities. Several works explaining this excess and neutrino electromagnetic properties can be found in the literature [22–31].

[*]krishnas542@gmail.com
[†]dinesh.sin.187@gmail.com
[‡]rmsp@uohyd.ac.in

Zwicky made a proposal in 1933 for the existence of dark matter through observations of spiral galaxy rotation curves; however, the physics of this mysterious particle is still unsettled. The freeze-out scenario has been the one that has fascinated theoretical physicists, a paradigm that is able to provide proper relic density as per the Planck satellite by a weakly interacting massive particle (WIMP). Now, we raise the question of whether a dark matter particle running in the loop and forming an electromagnetic vertex can provide a neutrino magnetic moment. With this viewpoint, we provide a simple model that can accommodate a nonzero magnetic moment for the neutrino and also discuss dark matter phenomenology in a correlative manner. We check the sensitivity of νMM with XENONnT [21], Borexino [32], TEXONO [33], Super-K [34], and white dwarfs [35] and also explain the excess in electron recoil events reported at XENON1T [20].

The paper is organized as follows: In Sec. II, we describe the model along with the particle content and interaction terms to address the neutrino magnetic moment, neutrino mass, and dark matter. The mass spectrum of the scalar sector due to mixing is also discussed in this section. Section III focuses on the neutrino magnetic moment and neutrino masses at one loop. Section IV describes the dark matter relic density and its detection prospects. Section V provides a detailed analysis, showing common parameter spaces to obtain observables related to the aspects of neutrino and dark matter sectors. We also emphasize more specific constraints on Yukawa couplings from current neutrino oscillation data. Section VI gives the signature of the magnetic moment in the light of electron recoil event excess at XENON1T and also the overall obtained range of the magnetic moment in the concerned model. Finally, concluding remarks are provided in Sec. VII.

II. MODEL DESCRIPTION

To address the neutrino mass, magnetic moment, and dark matter in a common platform, we extend the SM framework with three vectorlike fermion triplets Σ_k, with $k = 1, 2, 3$, and two inert scalar doublets η_j, with $j = 1, 2$. We impose an additional Z_2 symmetry to realize neutrino phenomenology at one loop and also for the stability of the dark matter candidate. The particle contents along with their charges are displayed in Table I.

TABLE I. Fields and their charges in the present model.

	Field	$SU(3)_C \times SU(2)_L \times U(1)_Y$	Z_2
Leptons	$\ell_L = (\nu, e)^T_L$	$(\mathbf{1}, \mathbf{2}, -1/2)$	+
	e_R	$(\mathbf{1}, \mathbf{1}, -1)$	+
	$\Sigma_{k(L,R)}$	$(1, \mathbf{3}, 0)$	−
Scalars	H	$(\mathbf{1}, \mathbf{2}, 1/2)$	+
	η_j	$(\mathbf{1}, \mathbf{2}, 1/2)$	−

The $SU(2)_L$ triplet $\Sigma_{L,R} = (\Sigma^1, \Sigma^2, \Sigma^3)^T_{L,R}$ can be expressed in the fundamental representation as

$$\Sigma_{L,R} = \frac{\sigma^a \Sigma^a_{L,R}}{\sqrt{2}} = \begin{pmatrix} \Sigma^0_{L,R}/\sqrt{2} & \Sigma^+_{L,R} \\ \Sigma^-_{L,R} & -\Sigma^0_{L,R}/\sqrt{2} \end{pmatrix}. \quad (1)$$

Here, σ^a's represent Pauli matrices, and $\Sigma^0_{L,R} = \Sigma^3_{L,R}$, $\Sigma^\pm_{L,R} = (\Sigma^1_{L,R} \mp \Sigma^2_{L,R})/\sqrt{2}$. The Lagrangian terms of the model are given by

$$\mathcal{L}_\Sigma = y'_{\alpha k} \overline{\ell_{\alpha L}} \Sigma_{kR} \tilde{\eta}_j + y_{\alpha k} \overline{\ell^c_{\alpha L}} i\sigma_2 \Sigma_{kL} \eta_j + \frac{i}{2} \mathrm{Tr}\left[\bar{\Sigma} \gamma^\mu D_\mu \Sigma\right] - \frac{1}{2} \mathrm{Tr}\left[\bar{\Sigma} M_\Sigma \Sigma\right] + \mathrm{H.c.} \quad (2)$$

In the above, $\Sigma^{+,0} = \Sigma^{+,0}_L + \Sigma^{+,0}_R$ and $\Sigma = (\Sigma_1, \Sigma_2, \Sigma_3)^T$. The covariant derivative for Σ is given by

$$D_\mu \Sigma = \partial_\mu \Sigma + ig \left[\sum_{a=1}^{3} \frac{\sigma^a}{2} W^a_\mu, \Sigma \right]. \quad (3)$$

The Lagrangian for the scalar sector takes the form

$$\mathcal{L}_{\mathrm{scalar}} = \left| \left(\partial_\mu + \frac{i}{2} g \sigma^a W^a_\mu + \frac{i}{2} g' B_\mu \right) \eta_1 \right|^2 + \left| \left(\partial_\mu + \frac{i}{2} g \sigma^a W^a_\mu + \frac{i}{2} g' B_\mu \right) \eta_2 \right|^2 - V(H, \eta_1, \eta_2), \quad (4)$$

where the inert doublets are denoted by $\eta_j = \binom{\eta^+_j}{\eta^0_j}$, with $\eta^0_j = \frac{\eta^R_j + i\eta^I_j}{\sqrt{2}}$, and the scalar potential is expressed as [36,37]

$$V(H, \eta_1, \eta_2) = \mu_H^2 H^\dagger H + \mu_1^2 \eta_1^\dagger \eta_1 + \mu_2^2 \eta_2^\dagger \eta_2 + \mu_{12}^2 (\eta_1^\dagger \eta_2 + \mathrm{H.c.}) + \lambda_H (H^\dagger H)^2 + \lambda_1 (\eta_1^\dagger \eta_1)^2 + \lambda_2 (\eta_2^\dagger \eta_2)^2 + \lambda_{12} (\eta_1^\dagger \eta_1)(\eta_2^\dagger \eta_2) + \lambda'_{12} (\eta_1^\dagger \eta_2)(\eta_2^\dagger \eta_1) + \frac{\lambda''_{12}}{2} \left[(\eta_1^\dagger \eta_2)^2 + \mathrm{H.c.} \right] + \sum_{j=1,2} \left(\lambda_{Hj} (H^\dagger H)(\eta_j^\dagger \eta_j) + \lambda'_{Hj} (H^\dagger \eta_j)(\eta_j^\dagger H) + \frac{\lambda''_{Hj}}{2} \left[(H^\dagger \eta_j)^2 + \mathrm{H.c.} \right] \right). \quad (5)$$

A. Copositive criteria

The above potential has a stable vacuum if [36]

$$\begin{aligned}
&\lambda_H, \lambda_1, \lambda_2 > 0,\\
&\lambda_{H1} + \lambda'_{H1} + 2\sqrt{\lambda_H \lambda_1} > 0,\\
&\lambda_{H2} + \lambda'_{H2} + 2\sqrt{\lambda_H \lambda_2} > 0,\\
&\lambda_{12} + \lambda'_{12} + 2\sqrt{\lambda_1 \lambda_2} > 0,\\
&|\lambda''_{H1}|, |\lambda''_{H2}|, |\lambda''_{12}| < |\lambda_H|, |\lambda_1|, |\lambda_2|, |\lambda_{H1}|, |\lambda'_{H1}|, |\lambda_{H2}|, |\lambda'_{H2}|, |\lambda_{12}|, |\lambda'_{12}|.
\end{aligned} \tag{6}$$

B. Mass spectrum

The mass matrices of the charged and neural scalar components are given by

$$\mathcal{M}_C^2 = \begin{pmatrix} \Lambda_{C1} & \mu_{12} \\ \mu_{12} & \Lambda_{C2} \end{pmatrix}, \qquad \mathcal{M}_R^2 = \begin{pmatrix} \Lambda_{R1} & \mu_{12} \\ \mu_{12} & \Lambda_{R2} \end{pmatrix},$$
$$\mathcal{M}_I^2 = \begin{pmatrix} \Lambda_{I1} & \mu_{12} \\ \mu_{12} & \Lambda_{I2} \end{pmatrix}. \tag{7}$$

Here,

$$\begin{aligned}
\Lambda_{Cj} &= \mu_j^2 + \frac{\lambda_{Hj}}{2} v^2,\\
\Lambda_{Rj} &= \mu_j^2 + \left(\lambda_{Hj} + \lambda'_{Hj} + \lambda''_{Hj}\right)\frac{v^2}{2},\\
\Lambda_{Ij} &= \mu_j^2 + \left(\lambda_{Hj} + \lambda'_{Hj} - \lambda''_{Hj}\right)\frac{v^2}{2}.
\end{aligned} \tag{8}$$

One can diagonalize the above mass matrices using $U_\theta = \left(\begin{smallmatrix} \cos\theta & \sin\theta \\ -\sin\theta & \cos\theta \end{smallmatrix}\right)$ as

$$\begin{aligned}
U_{\theta_C}^T \mathcal{M}_C^2 U_{\theta_C} &= \mathrm{diag}(M_{C1}^2, M_{C2}^2) \quad \text{with} \quad \theta_C = \tan^{-1}\left[\frac{2\mu_{12}^2}{\Lambda_{C2} - \Lambda_{C1}}\right],\\
U_{\theta_R}^T \mathcal{M}_R^2 U_{\theta_R} &= \mathrm{diag}(M_{R1}^2, M_{R2}^2) \quad \text{with} \quad \theta_R = \tan^{-1}\left[\frac{2\mu_{12}^2}{\Lambda_{R2} - \Lambda_{R1}}\right],\\
U_{\theta_I}^T \mathcal{M}_I^2 U_{\theta_I} &= \mathrm{diag}(M_{I1}^2, M_{I2}^2) \quad \text{with} \quad \theta_I = \tan^{-1}\left[\frac{2\mu_{12}^2}{\Lambda_{I2} - \Lambda_{I1}}\right].
\end{aligned} \tag{9}$$

The flavor and mass eigenstates can be related as

$$\begin{pmatrix} \eta_1^+ \\ \eta_2^+ \end{pmatrix} = U_{\theta_C}\begin{pmatrix} \phi_1^+ \\ \phi_2^+ \end{pmatrix}, \qquad \begin{pmatrix} \eta_1^R \\ \eta_2^R \end{pmatrix} = U_{\theta_R}\begin{pmatrix} \phi_1^R \\ \phi_2^R \end{pmatrix},$$
$$\begin{pmatrix} \eta_1^I \\ \eta_2^I \end{pmatrix} = U_{\theta_I}\begin{pmatrix} \phi_1^I \\ \phi_2^I \end{pmatrix}. \tag{10}$$

The invisible decays of Z and $W^\pm$ at LEP limit the masses of inert scalars as [38,39]

$$M_{Ci} > M_Z/2, \quad M_{Ri} + M_{Ii} > M_Z, \quad M_{Ci} + M_{Ri,Ii} > M_W. \tag{11}$$

Moving on to the fermion sector, electroweak radiative corrections provide a mass splitting of 166 MeV [40] between the charged and neutral components of the triplet. We work in the high-scale regime; this small splitting does not affect the phenomenology.

III. NEUTRINO PHENOMENOLOGY

A. Neutrino magnetic moment

Though the neutrino is electrically neutral, it can have electromagnetic interaction at loop level, as shown in Fig. 1, where $\psi(p)$ and $\psi(p')$ denote the incoming and outgoing neutrino states. The effective interaction Lagrangian takes the form [41]

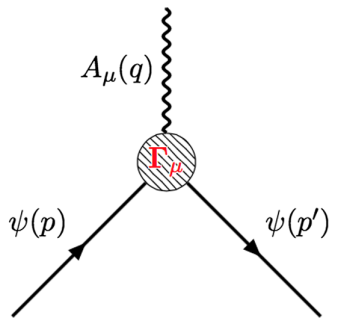

FIG. 1. Effective electromagnetic vertex, where $q = p - p'$.

$$\mathcal{L}_{\rm EM} = \bar{\psi}\Gamma_\mu \psi A^\mu. \tag{12}$$

In the above, the electromagnetic vertex function varies with the type of neutrino—i.e., Dirac or Majorana. In the case of a Dirac neutrino, Γ_μ takes the form

$$\Gamma_\mu(p,p') = f_Q(q^2)\gamma_\mu + if_M(q^2)\sigma_{\mu\nu}q^\nu + f_E(q^2)\sigma_{\mu\nu}q^\nu\gamma_5 + f_A(q^2)(q^2\gamma_\mu - q_\mu \not{q})\gamma_5, \tag{13}$$

where $f_Q(q^2)$, $f_M(q^2)$, $f_E(q^2)$, and $f_A(q^2)$ represent the form factors of the charge, magnetic dipole, electric dipole, and anapole, respectively.

In the nonrelativisitic regime, $f_Q(0) = Q$ stands for the charge, $f_M(0) = \mu$ represents the magnetic dipole moment, $f_E(0)$ denotes the electric dipole moment, and $f_A(0)$ stands for the Zeldovich anapole moment of the particle. All four form factors remain finite in a Dirac-type neutrino. For the Majorana case, using the property of charge conjugation $\psi^c = C\bar{\psi}^T$, we get

$$\bar{\psi}\Gamma_\mu\psi = \overline{\psi^c}\Gamma_\mu\psi^c = \overline{\psi}C\Gamma_\mu^T C^{-1}\psi. \tag{14}$$

Since $C\gamma_\mu^T C^{-1} = -\gamma_\mu$, $C(\gamma_\mu\gamma_5)^T C^{-1} = \gamma_\mu\gamma_5$, $C\sigma_{\mu\nu}^T C^{-1} = -\sigma_{\mu\nu}$, and $C(\sigma_{\mu\nu}\gamma_5)^T C^{-1} = -\sigma_{\mu\nu}\gamma_5$, we obtain

$$\Gamma_\mu(p,p') = -f_Q(q^2)\gamma_\mu - if_M(q^2)\sigma_{\mu\nu}q^\nu - f_E(q^2)\sigma_{\mu\nu}q^\nu\gamma_5 + f_A(q^2)(q^2\gamma_\mu - q_\mu \not{q})\gamma_5, \tag{15}$$

which results in $f_Q(q^2) = f_M(q^2) = f_E(q^2) = 0$ for a Majorana neutrino. However, if the electromagnetic current is between two different neutrino flavors in the initial and final states—i.e., $\overline{\psi_i}\Gamma_\mu\psi_j A^\mu$ with $i \neq j$—Majorana neutrinos can have nonzero transition dipole moments.

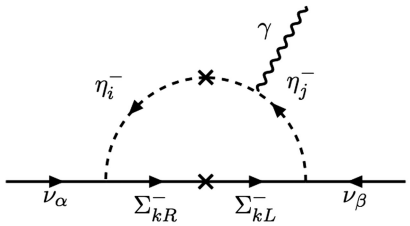

FIG. 2. One-loop Feynman diagram for transition magnetic moment.

In the present model, the magnetic moment arises from the one-loop diagram shown in Fig. 2, and the expression of corresponding contribution takes the form [42]

$$(\mu_\nu)_{\alpha\beta} = \sum_{k=1}^{3}\frac{(Y^2)_{\alpha\beta}}{8\pi^2}M_{\Sigma_k^+}\left[(1+\sin 2\theta_C)\frac{1}{M_{C2}^2}\left(\ln\left[\frac{M_{C2}^2}{M_{\Sigma_k^+}^2}\right]-1\right) + (1-\sin 2\theta_C)\frac{1}{M_{C1}^2}\left(\ln\left[\frac{M_{C1}^2}{M_{\Sigma_k^+}^2}\right]-1\right)\right], \tag{16}$$

where $y = y' = Y$ and $(Y^2)_{\alpha\beta} = Y_{\alpha k}Y_{k\beta}^T$.

B. Neutrino mass

In the present model, contribution to neutrino mass can arise at one loop from two diagrams—one with charged scalars and fermion triplets in the loop, while the other has neutral scalars and fermion triplets. The relevant diagrams are provided in Fig. 3, and the corresponding contribution takes the form [43–45]

$$\begin{aligned}(\mathcal{M}_\nu)_{\alpha\beta} = &\sum_{k=1}^{3}\frac{(Y^2)_{\alpha\beta}}{32\pi^2}M_{\Sigma_k^+}\left[(1+\sin 2\theta_C)\frac{M_{C2}^2}{M_{\Sigma_k^+}^2-M_{C2}^2}\ln\left(\frac{M_{\Sigma_k^+}^2}{M_{C2}^2}\right)+(1-\sin 2\theta_C)\frac{M_{C1}^2}{M_{\Sigma_k^+}^2-M_{C1}^2}\ln\left(\frac{M_{\Sigma_k^+}^2}{M_{C1}^2}\right)\right]\\ &+\sum_{k=1}^{3}\frac{(Y^2)_{\alpha\beta}}{32\pi^2}M_{\Sigma_k^0}\left[(1+\sin 2\theta_R)\frac{M_{R2}^2}{M_{\Sigma_k^0}^2-M_{R2}^2}\ln\left(\frac{M_{\Sigma_k^0}^2}{M_{R2}^2}\right)+(1-\sin 2\theta_R)\frac{M_{R1}^2}{M_{\Sigma_k^0}^2-M_{R1}^2}\ln\left(\frac{M_{\Sigma_k^0}^2}{M_{R1}^2}\right)\right]\\ &-\sum_{k=1}^{3}\frac{(Y^2)_{\alpha\beta}}{32\pi^2}M_{\Sigma_k^0}\left[(1+\sin 2\theta_I)\frac{M_{I2}^2}{M_{\Sigma_k^0}^2-M_{I2}^2}\ln\left(\frac{M_{\Sigma_k^0}^2}{M_{I2}^2}\right)+(1-\sin 2\theta_I)\frac{M_{I1}^2}{M_{\Sigma_k^0}^2-M_{I1}^2}\ln\left(\frac{M_{\Sigma_k^0}^2}{M_{I1}^2}\right)\right].\end{aligned} \tag{17}$$

IV. DARK MATTER PHENOMENOLOGY

A. Relic density

The model provides scalar dark matter candidates, and we study their phenomenology for dark matter masses up to the 2 TeV range. All the inert scalar components contribute to the dark matter density of the Universe through annihilations and coannihilations. With the mediation of scalar

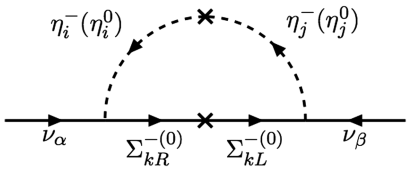

FIG. 3. One-loop diagram that generates light neutrino mass.

Higgs, $\phi_i^R\phi_j^R$ can annihilate to $f\bar{f}$, W^+W^-, ZZ, hh, and via the Z boson, $\phi_i^R\phi_j^I$ can coannihilate to $f\bar{f}$, W^+W^-, and Zh. The charged and neutral components can coannihilate to $f'\overline{f''}$, $AW^\pm$, $ZW^\pm$, and $hW^\pm$ through $W^\pm$. Here, $f' = u, c, t, \nu_e, \nu_\mu, \nu_\tau$, and $f'' = d, s, b, e, \mu, \tau$ [46–48]. The abundance of dark matter can be computed by

$$\Omega h^2 = \frac{1.07 \times 10^9 \text{ GeV}^{-1}}{M_{\text{Pl}} {g_*}^{1/2}} \frac{1}{J(x_f)}, \tag{18}$$

where $M_{\text{Pl}} = 1.22 \times 10^{19}$ GeV and $g_* = 106.75$ denote the Planck mass and the total number of effective relativistic degrees of freedom, respectively. The function J is

$$J(x_f) = \int_{x_f}^{\infty} \frac{\langle \sigma v \rangle(x)}{x^2} dx. \tag{19}$$

In the above, the thermally averaged cross section $\langle \sigma v \rangle$ reads as

$$\langle \sigma v \rangle(x) = \frac{x}{8M_{\text{DM}}^5 K_2^2(x)} \int_{4M_{\text{DM}}^2}^{\infty} \hat{\sigma} \times (s - 4M_{\text{DM}}^2)\sqrt{s} K_1 \times \left(\frac{x\sqrt{s}}{M_{\text{DM}}}\right) ds. \tag{20}$$

Here K_1, K_2 are the modified Bessel functions, $x = M_{\text{DM}}/T$, where T is the temperature, M_{DM} is the dark matter mass, $\hat{\sigma}$ is the dark matter cross section, and x_f stands for the freeze-out parameter.

B. Direct searches

Moving to direct searches, the scalar dark matter can scatter off the nucleus via the Higgs and the Z boson. Mass splitting between real and imaginary components above 100 KeV can forbid gauge kinematics [48]. Thus, the DM-nucleon cross section in the Higgs portal can provide a spin-independent (SI) cross section, whose sensitivity can be checked with a stringent upper bound of the LZ-ZEPLIN experiment. The effective interaction Lagrangian in the Higgs portal takes the form

$$\begin{aligned} &\mathcal{L}_{\text{eff}} = a_q \phi_1^R \phi_1^R q\bar{q}, \quad \text{where} \\ &a_q = \frac{M_q}{2M_h^2 M_{R1}} \left(\lambda_{L1} \cos^2\theta_R + \lambda_{L2} \sin^2\theta_R\right) \quad \text{with} \\ &\lambda_{Lj} = \lambda_{Hj} + \lambda'_{Hj} + \lambda''_{Hj}. \end{aligned} \tag{21}$$

The corresponding cross section is given by [46–48]

$$\sigma_{\text{SI}} = \frac{1}{4\pi} \left(\frac{M_n M_{R1}}{M_n + M_{R1}}\right)^2 \left(\frac{\lambda_{L1} \cos^2\theta_R + \lambda_{L2} \sin^2\theta_R}{2M_{R1} M_h^2}\right)^2 f^2 M_n^2, \tag{22}$$

where M_n denotes the nucleon mass, and the nucleonic matrix element $f \sim 0.3$ [49]. We have implemented the model in the LanHEP [50] package and used micrOMEGAs [51–53] to compute relic density and also the DM-nucleon cross section. The detailed analysis of neutrino and dark matter observables and their viability through a common parameter space will be discussed in the upcoming section.

V. ANALYSIS

In the present framework, we consider ϕ_1^R to be the lightest inert scalar eigenstate, and there are five other heavier scalars. To make the analysis simpler, we consider the mass parameters related to the scalar masses as follows: one parameter M_{R1} corresponding to the mass of ϕ_1^R, and three mass splittings—namely δ, δ_{IR}, and δ_{CR}. The masses of the rest of the inert scalars can be derived using the following relations:

$$\begin{aligned} &M_{R2} - M_{R1} = M_{I2} - M_{I1} = M_{C2} - M_{C1} = \delta, \\ &M_{Ri} - M_{Ii} = \delta_{\text{IR}}, \qquad M_{Ri} - M_{Ci} = \delta_{\text{CR}}, \end{aligned} \tag{23}$$

where $i = 1, 2$. In the above setup, the scalar mixing angles can be related as follows:

$$\sin 2\theta_I = \sin 2\theta_R \left(\frac{2M_{R1} + \delta}{2M_{R1} + 2\delta_{\text{IR}} + \delta}\right), \tag{24}$$

$$\sin 2\theta_C = \sin 2\theta_R \left(\frac{2M_{R1} + \delta}{2M_{R1} + 2\delta_{\text{CR}} + \delta}\right). \tag{25}$$

We have performed the scan over model parameters as given below in order to obtain the region, consistent with experimental bounds associated with both dark matter and neutrino sectors:

$$\begin{aligned} &100 \text{ GeV} \le M_{R1} \le 2000 \text{ GeV}, \qquad 0 \le \sin\theta_R \le 1, \\ &0.1 \text{ GeV} \le \delta < 200 \text{ GeV}, \\ &0.1 \text{ GeV} \le \delta_{\text{IR}}, \delta_{\text{CR}} \le 20 \text{ GeV}. \end{aligned} \tag{26}$$

We filter out the parameter space by providing the Planck constraint on relic density [54] in 3σ and then compute the DM-nucleon SI cross section for the available parameter space. We project the cross section as a function of M_{R1} in the left panel of Fig. 4 with cyan data points, where the dashed brown line corresponds to the LZ-ZEPLIN upper limit [55]. Choosing a set of values for the Yukawa and fermion triplet mass, with the obtained parameter space, one can satisfy the discussed aspects of neutrino phenomenology. The blue, green, and red data points corresponding to 25, 80, and 420 TeV of the triplet mass and suitable Yukawa satisfy the neutrino magnetic moment and light neutrino mass in the desired range simultaneously, as projected in the right panel. We notice that a wide region

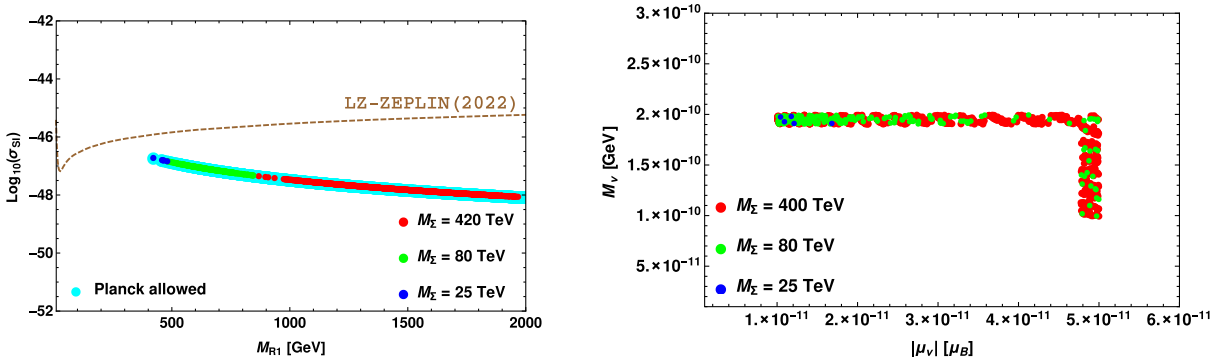

FIG. 4. Left panel projects the SI WIMP-nucleon cross section as a function M_{R1}, with the dashed brown line showing the LZ-ZEPLIN upper limit [55]. Cyan data points satisfy the Planck limit [54] on relic abundance in 3σ. Blue, green, and red data points satisfy neutrino mass and magnetic moment for a specific set of values for a fermion triplet and Yukawa, visible in the right panel.

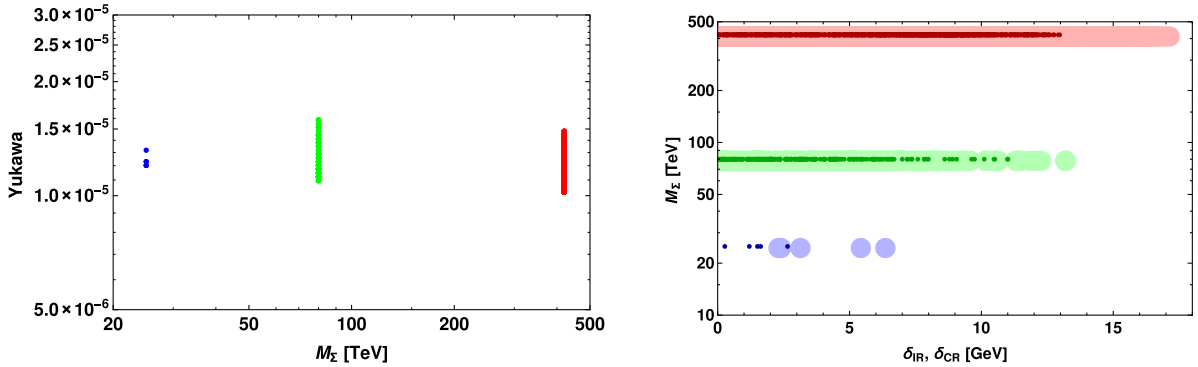

FIG. 5. Left panel displays the suitable region for the triplet mass and Yukawa to explain neutrino phenomenology. Right panel shows the allowed region for scalar mass splittings; thick (thin) bands correspond to $\delta_{\rm IR}$ ($\delta_{\rm CR}$).

of dark matter mass is favored as we move towards high scale (triplet mass), and moreover, the favorable region shifts toward larger values with scale. The suitable region of the Yukawa and fermion triplet mass is depicted in the left panel of Fig. 5, with the allowed range for scalar mass splittings displayed in the right panel. Here, the light-colored band corresponds to $\delta_{\rm IR}$, and the dark-colored band stands for $\delta_{\rm CR}$. Using two specific benchmark values (shown in Tables II and III) which are favorable to explain both the neutrino and dark matter aspects discussed so far, we project the relic abundance of scalar dark matter in Fig. 6.

A. Constraints from neutrino oscillation parameters

More specific constraints on the Yukawa couplings can be obtained from the neutrino oscillation parameters. For this purpose, we consider the neutrino mixing matrix as the

TABLE II. Set of benchmarks from the consistent parameter space.

	M_{R1} [GeV]	δ [GeV]	$\delta_{\rm CR}$ [GeV]	$\delta_{\rm IR}$ [GeV]	M_Σ [TeV]	Yukawa	$\sin\theta_R$
Benchmark 1	1472	101.69	9.03	0.35	420	$10^{-4.89}$	0.09
Benchmark 2	628	36.40	4.38	3.45	80	$10^{-4.85}$	0.06

TABLE III. Neutrino and dark matter observables for the given benchmarks.

	$\lvert\mu_\nu\rvert$ [μ_B]	$\mathcal{M}_\nu$ [GeV]	Log$_{10}^{[\sigma_{\rm SI}]}$ cm^{-2}	Ωh^2
Benchmark 1	2.73×10^{-11}	1.99×10^{-10}	−47.78	0.123
Benchmark 2	3.03×10^{-11}	1.92×10^{-10}	−47.04	0.119

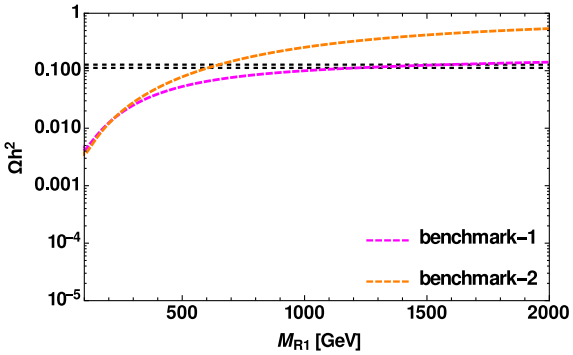

FIG. 6. Relic density as a function of dark matter mass for the chosen benchmark of the favorable parameter space of Table II.

product of a tri-bimaximal (TBM) matrix with a rotation matrix U_{13}, given by

$$U_\nu = U_{\rm TBM}\cdot U_{13} = \begin{pmatrix} \cos\Theta & \sin\Theta & 0 \\ -\frac{\sin\Theta}{\sqrt{2}} & \frac{\cos\Theta}{\sqrt{2}} & \frac{1}{\sqrt{2}} \\ \frac{\sin\Theta}{\sqrt{2}} & -\frac{\cos\Theta}{\sqrt{2}} & \frac{1}{\sqrt{2}} \end{pmatrix} \cdot \begin{pmatrix} \cos\varphi & 0 & e^{-i\zeta}\sin\varphi \\ 0 & 1 & 0 \\ -e^{i\zeta}\sin\varphi & 0 & \cos\varphi \end{pmatrix}. \quad (27)$$

From Eqs. (16) and (17), the matrices associated with neutrino magnetic moment and mass can be written in a compact form as

$$\mu_\nu = Y\cdot \mathrm{diag}(\Lambda_1,\Lambda_2,\Lambda_3)\cdot Y^T,$$
$$\mathcal{M}_\nu = Y\cdot \mathrm{diag}(\Lambda_1',\Lambda_2',\Lambda_3')\cdot Y^T, \quad (28)$$

where

$$\Lambda_k = \frac{1}{8\pi^2} M_{\Sigma_k^+}\left[(1+\sin 2\theta_C)\frac{1}{M_{C2}^2}\left(\ln\left[\frac{M_{C2}^2}{M_{\Sigma_k^+}^2}\right]-1\right)+(1-\sin 2\theta_C)\frac{1}{M_{C1}^2}\left(\ln\left[\frac{M_{C1}^2}{M_{\Sigma_k^+}^2}\right]-1\right)\right],$$

$$\begin{aligned}\Lambda_k' = \frac{1}{32\pi^2} M_{\Sigma_k^+}\Bigg(&\left[(1+\sin 2\theta_C)\frac{M_{C2}^2}{M_{\Sigma_k^+}^2-M_{C2}^2}\ln\left(\frac{M_{\Sigma_k^+}^2}{M_{C2}^2}\right)+(1-\sin 2\theta_C)\frac{M_{C1}^2}{M_{\Sigma_k^+}^2-M_{C1}^2}\ln\left(\frac{M_{\Sigma_k^+}^2}{M_{C1}^2}\right)\right]\\ &+\left[(1+\sin 2\theta_R)\frac{M_{R2}^2}{M_{\Sigma_k^0}^2-M_{R2}^2}\ln\left(\frac{M_{\Sigma_k^0}^2}{M_{R2}^2}\right)+(1-\sin 2\theta_R)\frac{M_{R1}^2}{M_{\Sigma_k^0}^2-M_{R1}^2}\ln\left(\frac{M_{\Sigma_k^0}^2}{M_{R1}^2}\right)\right]\\ &-\left[(1+\sin 2\theta_I)\frac{M_{I2}^2}{M_{\Sigma_k^0}^2-M_{I2}^2}\ln\left(\frac{M_{\Sigma_k^0}^2}{M_{I2}^2}\right)+(1-\sin 2\theta_I)\frac{M_{I1}^2}{M_{\Sigma_k^0}^2-M_{I1}^2}\ln\left(\frac{M_{\Sigma_k^0}^2}{M_{I1}^2}\right)\right]\Bigg),\end{aligned} \quad (29)$$

and

$$Y = \begin{pmatrix} Y_{e1} & Y_{e2} & Y_{e3} \\ Y_{\mu 1} & Y_{\mu 2} & Y_{\mu 3} \\ Y_{\tau 1} & Y_{\tau 2} & Y_{\tau 3} \end{pmatrix}. \quad (30)$$

Diagonalizing the matrices in Eq. (28) using U_ν, we obtain three unique solutions where the Yukawa couplings corresponding to different flavors become linearly dependent. The relations take the form

$$\begin{aligned} Y_{e1} &= \left(\frac{\sqrt{2}\cos\Theta\cos\varphi}{\sin\Theta\cos\varphi - e^{-i\zeta}\sin\varphi}\right)Y_{\tau 1}, \qquad Y_{e2} = -\frac{\sqrt{2}\sin\Theta}{\cos\Theta}Y_{\tau 2}, \qquad Y_{e3} = \left(\frac{\sqrt{2}\cos\Theta\sin\varphi}{\sin\Theta\sin\varphi + e^{-i\zeta}\cos\varphi}\right)Y_{\tau 3},\\ Y_{\mu 1} &= \left(\frac{e^{-i\zeta}\sin\varphi + \sin\Theta\cos\varphi}{e^{-i\zeta}\sin\varphi - \sin\Theta\cos\varphi}\right)Y_{\tau 1}, \qquad Y_{\mu 2} = -Y_{\tau 2}, \qquad Y_{\mu 3} = \left(\frac{e^{-i\zeta}\cos\varphi - \sin\Theta\sin\varphi}{e^{-i\zeta}\cos\varphi + \sin\Theta\sin\varphi}\right)Y_{\tau 3}. \end{aligned} \quad (31)$$

Thus, the obtained diagonalized matrices associated with neutrino magnetic moment and mass in the basis of active neutrinos are [56–58]

$$\mu_\nu^D = \begin{pmatrix} a_1(Y_{\tau 1}^2\Lambda_1) & 0 & 0 \\ 0 & a_2(Y_{\tau 2}^2\Lambda_2) & 0 \\ 0 & 0 & a_3(Y_{\tau 3}^2\Lambda_3) \end{pmatrix},$$
$$\mathcal{M}_\nu^D = \begin{pmatrix} a_1(Y_{\tau 1}^2\Lambda_1') & 0 & 0 \\ 0 & a_2(Y_{\tau 2}^2\Lambda_2') & 0 \\ 0 & 0 & a_3(Y_{\tau 3}^2\Lambda_3') \end{pmatrix}, \quad (32)$$

where

$$a_1 = \frac{2e^{2i\zeta}}{(-e^{i\zeta}\cos\varphi\sin\Theta + \sin\varphi)^2}, \qquad a_2 = \frac{2}{\cos^2\Theta},$$
$$a_3 = \frac{2e^{-2i\zeta}}{(e^{-i\zeta}\cos\varphi + \sin\Theta\sin\varphi)^2}. \quad (33)$$

The matrix U_ν replicates the standard Pontecorvo-Maki-Nakagawa-Sakata (PMNS) matrix, where the mixing angles, Θ and φ, can be fixed using the observed neutrino oscillation parameters. Using the best-fit values on θ_{12}, θ_{13}, and θ_{23} from [59], we get $\Theta = 33.04°$ and $\varphi = 10.18°$. Furthermore, we take $\zeta = 180°$, which falls within the 1σ region of the observed value of CP phase 197^{+27}_{-24} [59]. Substituting the above, we get

$$|U_\nu| = \begin{pmatrix} 0.8250 & 0.5452 & 0.1481 \\ 0.2544 & 0.5927 & 0.7641 \\ 0.5044 & 0.5927 & 0.6278 \end{pmatrix}, \quad (34)$$

which is consistent enough in comparison with the leptonic mixing matrix that it can explain the observed mixing angles in the 3σ region [59]:

$$|U_{\rm PMNS}^{\rm SK-3\sigma}| = \begin{pmatrix} 0.801 \to 0.845 & 0.513 \to 0.579 & 0.143 \to 0.155 \\ 0.234 \to 0.500 & 0.471 \to 0.689 & 0.637 \to 0.776 \\ 0.271 \to 0.525 & 0.477 \to 0.694 & 0.613 \to 0.756 \end{pmatrix}. \quad (35)$$

Furthermore, the Yukawa matrix turns out to be

$$Y = \begin{pmatrix} 1.6356Y_{\tau 1} & -0.9197Y_{\tau 2} & -0.2360Y_{\tau 3} \\ -0.5044Y_{\tau 1} & -Y_{\tau 2} & 1.2170Y_{\tau 3} \\ Y_{\tau 1} & Y_{\tau 2} & Y_{\tau 3} \end{pmatrix}, \quad (36)$$

and the relevant coefficients in the diagonal matrices of Eq. (32) become $a_1 = 3.930$, $a_2 = 2.846$, and $a_3 = 2.537$.

To illustrate, we consider all three generations of heavy fermion triplets to be degenerate in mass—i.e., $m_\Sigma \sim 420$ TeV—and scan the DM consistent parameter space to extract the constraints on Yukawa. In Fig. 7, we project the allowed region of Yukawa (shown as cyan, magenta, and orange data points) that satisfies the required bound on mass squared differences [59] in 3σ (blue and black dashed lines), and also the cosmological bound on the sum of active neutrino masses—i.e., $0.058 \le (m_1 + m_2 + m_3) \le 0.12$ eV (normal hierarchy) [60], represented as green vertical lines. We mention that this projected parameter space is consistent with the neutrino magnetic moment in a wide range of values—i.e., 3×10^{-12} to 7×10^{-10} (in units of μ_B)—which is the regime where all the experiments have provided the bounds (to be discussed in the next section).

VI. IMPLICATIONS

In the experimental perspective, a nonzero neutrino magnetic moment of solar neutrinos can provide an explanation for the excess in electron recoil events at the XENON1T Collaboration [20]. In other words, the neutrino transition magnetic moment can provide an additional contribution to the neutrino-electron scattering process. In this section, we utilize a nonzero transition neutrino magnetic moment to explain the excess in electron recoil events.

In the presence of magnetic moment, the total differential cross section can be written as [61]

$$\left(\frac{d\sigma}{dT_e}\right)_{\rm TOT} = \left(\frac{d\sigma}{dT_e}\right)_{\rm SM} + \left(\frac{d\sigma}{dT_e}\right)_{\rm EM}, \quad (37)$$

where T_e is the electron recoil energy. The first contribution in Eq. (37) is due to standard weak interactions, given by

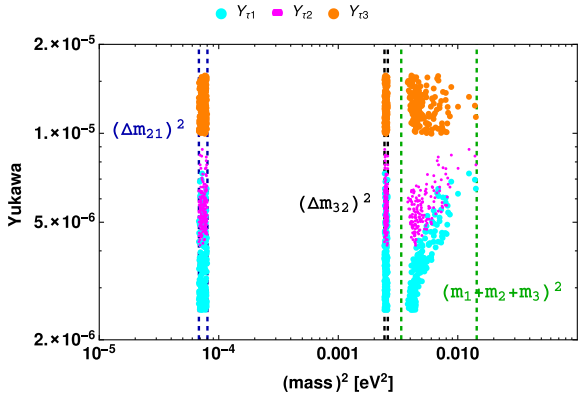

FIG. 7. Allowed region of Yukawa (colored data points), satisfying the 3σ limit on mass-squared differences [59] and cosmological bounds on the sum of active neutrino masses [60] (colored vertical lines).

$$\left(\frac{d\sigma}{dT_e}\right)_{\rm SM} = \frac{G_F^2 m_e}{2\pi}\left[(g_V+g_A)^2+\left(1-\frac{T_e}{E_\nu}\right)^2(g_V-g_A)^2 + \left(\frac{m_e T_e}{E_\nu^2}\right)(g_A^2-g_V^2)\right]. \quad (38)$$

In the above, G_F stands for the Fermi constant, and

$$g_V = 2\sin^2\theta_W + \frac{1}{2}, \qquad g_A = 1/2 \quad \text{for } \nu_e,$$
$$g_V = 2\sin^2\theta_W - \frac{1}{2}, \qquad g_A = -1/2 \quad \text{for } \nu_\mu, \nu_\tau. \quad (39)$$

The second contribution comes from the effective electromagnetic vertex of the neutrinos—i.e., the magnetic moment contribution, which is expressed as

$$\left(\frac{d\sigma}{dT_e}\right)_{\rm EM} = \frac{\pi\alpha^2}{m_e^2}\left(\frac{1}{T_e}-\frac{1}{E_\nu}\right)\left(\frac{\mu_{\nu_{e\mu}}}{\mu_B}\right)^2, \quad (40)$$

where α is the electromagnetic coupling, E_ν is the initial neutrino energy, $\mu_{\nu_{e\mu}}$ is the neutrino magnetic moment, and μ_B is the Bohr magneton. For high T_e values, the weak cross-section dominates, and for low T_e values, the electromagnetic cross section dominates, and hence we search for the signature of the neutrino magnetic moment in the low-energy region. For simplicity, we take one transition magnetic moment $\mu_{\nu_{e\mu}}$ to explain the XENON1T excess. The differential event rate to estimate the XENON1T signal is given by

$$\frac{dN}{dT_r} = n_{\rm te}\times\int_{E_\nu^{\rm min}}^{E_\nu^{\rm max}} dE_\nu \int_{T_{\rm th}}^{T_{\rm max}} dT_e\left(\frac{d\sigma^{\nu_e e}}{dT_e}P_{ee} + \cos^2\theta_{23}\frac{d\sigma^{\nu_\mu e}}{dT_e}P_{e\mu}\right)\times\frac{d\phi_s}{dE_\nu}\times\varepsilon(T_e)\times G(T_e,T_r). \quad (41)$$

In the above, $\varepsilon(T_e)$ denotes the efficiency of the detector [20], n_{te} is the count of target electrons in the fiducial volume of one ton of xenon [62], $d\phi_s/dE_\nu$ represents the solar neutrino flux spectrum [63], and the function $G(T_e,T_r)$ reflects the normalized Gaussian smearing function that takes into account the detector's limited energy resolution [20]. The limits $T_{\rm th}=1$ KeV and $T_{\rm max}=30$ KeV stand for the threshold and maximum recoil energy of the detector, respectively. The extremes of neutrino energy for the integral are given by $E_\nu^{\rm max}=420$ KeV and $E_\nu^{\rm min}=[T+(2m_eT+T^2)^{\frac{1}{2}}]/2$ [42]. The survival probability can be expressed as

$$P_{ee} = \sin^4\theta_{13} + \frac{1}{2}\cos^4\theta_{13}(1+\cos 2\theta_{12}^m + \cos 2\theta_{12}), \quad (42)$$

and the disappearance probability can be taken as $P_{e\mu/\tau} = 1-P_{ee}$ [64,65]. The oscillation parameters are taken from [59]. In Fig. 8, we project the event rate as a function of recoil energy T_r, for two sets of values for magnetic moment—i.e., $\mu_{\nu_{e\mu}} = 2.6\times10^{-11}\mu_B$ and $3.2\times10^{-11}\mu_B$ (red curves). Adding the background (green curve), we are able to meet the observed recoil event excess in the low-energy region near 2.5 KeV as of the XENON1T experiment [20].

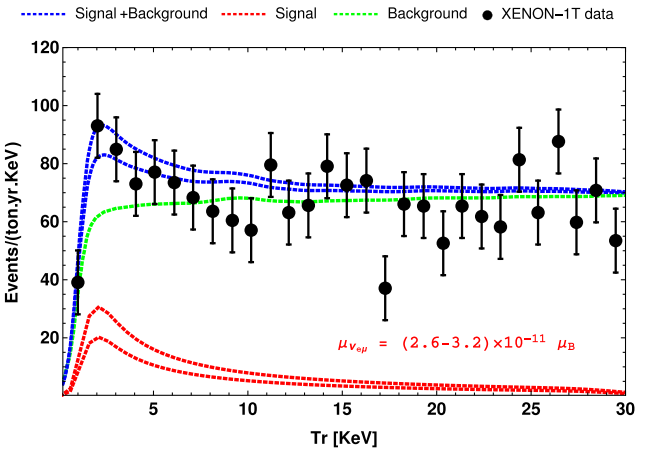

FIG. 8. Excess recoil events (blue) to match XENON1T [20] (black) through the signal from the transition neutrino magnetic moment $\mu_{\nu_{e\mu}} = 2.6\times10^{-11}\mu_B$ and $3.2\times10^{-11}\mu_B$ (in red) along with the background (green).

In Fig. 9, we project the neutrino magnetic moment as a function of dark matter mass, choosing specific set of values assigned to the triplet fermion. As seen earlier in the left panel of Fig. 4, a specific range of dark matter mass is favored with the scale of triplet mass. It is transparent that the model parameters are able to provide a neutrino magnetic moment in the range $10^{-12}\mu_B$ to $10^{-10}\mu_B$, sensitive to the upper limits of Super-K [34], TEXONO [33], Borexino [32],

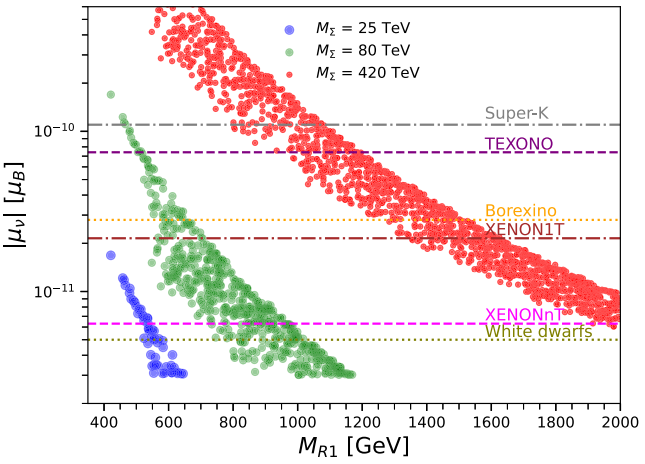

FIG. 9. Allowed region of neutrino magnetic moment with the mass spectrum of dark matter and fermion triplet. Horizontal colored lines stand for the upper bounds of XENON1T (average value of suggested range in [20]), XENONnT [21], Borexino [32], TEXONO [33], Super-K [34], and white dwarfs [35].

XENON1T [20], XENONnT [21], and white dwarfs [35] (colored horizontal lines). Thus, from all the above discussions, it is evident that this simple framework can provide a consistent phenomenological platform for a correlative study of neutrino magnetic moment (especially), mass, and dark matter physics.

VII. CONCLUDING REMARKS

The primary aim is to address neutrino mass, magnetic moment, and dark matter phenomenology in a common framework. For this purpose, we have extended the standard model with three vectorlike fermion triplets and two inert scalar doublets to realize a Type-III radiative scenario. A pair of charged scalars help in obtaining the neutrino magnetic moment; all charged and neutral scalars get a light neutrino mass at the one-loop level. All the inert scalars participate in annihilation and coannihilation channels to provide the total dark matter relic density of the Universe, consistent with Planck satellite data, and also provide a suitable cross section with nucleons sensitive to the LZ-ZEPLIN upper limit. The lightest dark matter mass is scanned up to 2 TeV, while the fermion triplet mass is taken with larger values—i.e., a few hundred TeV. Choosing Yukawa of the order 10^{-5}, we have obtained a light neutrino mass in the sub-eV scale and also a transition magnetic moment of $\sim 10^{-11}\ \mu_B$, to successfully explain the excess electron recoil events at a low-energy scale reported by the XENON1T experiment. Finally, we have also demonstrated with a plot that the model is able to provide the neutrino magnetic moment in a wide range ($10^{-12}\mu_B$ to $10^{-10}\mu_B$), in the same ball park as Borexino, Super-K, TEXONO, XENONnT, and white dwarfs. Overall, this simple model provides a suitable platform to study neutrino phenomenology, especially the neutrino magnetic moment and also dark matter aspects.

ACKNOWLEDGMENTS

S. S. and R. M. would like to acknowledge University of Hyderabad IoE project Grant No. RC1-20-012. D. K. S. would like to acknowledge the Prime Minister's Research Fellowship, Government of India. S. S. would like to thank Dr. Siddhartha Karmakar and Papia Panda for helpful input in the work.

[1] S. M. Bilenky, in *Proceedings of the 1999 European School of High-Energy Physics* (CERN Yellow Reports, Geneva, 1999), pp. 187–217, arXiv:hep-ph/0001311.
[2] R. N. Mohapatra and G. Senjanovic, Phys. Rev. Lett. **44**, 912 (1980).
[3] J. Schechter and J. W. F. Valle, Phys. Rev. D **22**, 2227 (1980).
[4] K. Babu and R. Mohapatra, Phys. Rev. Lett. **70**, 2845 (1993).
[5] J. Hosaka *et al.* (Super-Kamiokande Collaboration), Phys. Rev. D **73**, 112001 (2006).
[6] Q. R. Ahmad *et al.* (SNO Collaboration), Phys. Rev. Lett. **89**, 011301 (2002).
[7] K. Abe *et al.* (Super-Kamiokande Collaboration), Phys. Rev. D **94**, 052010 (2016).
[8] K. Abe *et al.* (T2K Collaboration), Phys. Rev. D **99**, 071103 (2019).
[9] F. P. An *et al.* (Daya Bay Collaboration), Phys. Rev. Lett. **108**, 171803 (2012).
[10] Y. Abe *et al.* (Double Chooz Collaboration), Phys. Rev. Lett. **108**, 131801 (2012).
[11] F. Zwicky, Astrophys. J. **86**, 217 (1937).
[12] F. Zwicky, Phys. Rev. **43**, 147 (1933).
[13] G. Bertone, D. Hooper, and J. Silk, Phys. Rep. **405**, 279 (2005).
[14] Y. Mambrini, N. Nagata, K. A. Olive, J. Quevillon, and J. Zheng, Phys. Rev. D **91**, 095010 (2015).
[15] A. Sakharov, Sov. Phys. Usp. **34**, 392 (1991).
[16] E. W. Kolb and S. Wolfram, Nucl. Phys. **B172**, 224 (1980); **B195**, 542(E) (1982).
[17] M. Fukugita and T. Yanagida, Phys. Lett. B **174**, 45 (1986).
[18] H. Fritzsch and P. Minkowski, Ann. Phys. (N.Y.) **93**, 193 (1975).
[19] S. Bifani, S. Descotes-Genon, A. Romero Vidal, and M.-H. Schune, J. Phys. G **46**, 023001 (2019).
[20] E. Aprile *et al.* (XENON Collaboration), Phys. Rev. D **102**, 072004 (2020).
[21] E. Aprile *et al.* (XENON Collaboration), Phys. Rev. Lett. **129**, 161805 (2022).
[22] O. G. Miranda, D. K. Papoulias, M. Tórtola, and J. W. F. Valle, Phys. Lett. B **808**, 135685 (2020).
[23] Y.-F. Li and S.-y. Xia, Phys. Rev. D **106**, 095022 (2022).
[24] O. G. Miranda, D. K. Papoulias, O. Sanders, M. Tórtola, and J. W. F. Valle, J. High Energy Phys. 12 (2021) 191.
[25] K. S. Babu, S. Jana, M. Lindner, and V. P. K, J. High Energy Phys. 10 (2021) 240.
[26] V. Brdar, A. Greljo, J. Kopp, and T. Opferkuch, J. Cosmol. Astropart. Phys. 01 (2021) 039.
[27] A. N. Khan, Phys. Lett. B **837**, 137650 (2023).
[28] A. N. Khan, Nucl. Phys. **B986**, 116064 (2023).
[29] J. Jeong, J. E. Kim, and S. Youn, Int. J. Mod. Phys. A **36**, 2150182 (2021).
[30] A. K. Alok, N. R. Singh Chundawat, and A. Mandal, Phys. Lett. B **839**, 137791 (2023).
[31] J. A. Dror, G. Elor, R. McGehee, and T.-T. Yu, Phys. Rev. D **103**, 035001 (2021); **105**, 119903(E) (2022).

[32] M. Agostini *et al.* (Borexino Collaboration), Phys. Rev. D **96**, 091103 (2017).
[33] H. T. Wong *et al.* (TEXONO Collaboration), Phys. Rev. D **75**, 012001 (2007).
[34] D. W. Liu *et al.* (Super-Kamiokande Collaboration), Phys. Rev. Lett. **93**, 021802 (2004).
[35] M. M. Miller Bertolami, Astron. Astrophys. **562**, A123 (2014).
[36] V. Keus, S. F. King, S. Moretti, and D. Sokolowska, J. High Energy Phys. 11 (2014) 016.
[37] V. Keus, S. F. King, and S. Moretti, Phys. Rev. D **90**, 075015 (2014).
[38] Q.-H. Cao, E. Ma, and G. Rajasekaran, Phys. Rev. D **76**, 095011 (2007).
[39] E. Lundstrom, M. Gustafsson, and J. Edsjo, Phys. Rev. D **79**, 035013 (2009).
[40] M. Cirelli, N. Fornengo, and A. Strumia, Nucl. Phys. **B753**, 178 (2006).
[41] Z.-z. Xing and S. Zhou, *Neutrinos in Particle Physics, Astronomy and Cosmology* (Springer, Berlin, 2011), ISBN 978-3-642-17559-6, 978-7-308-08024-8.
[42] K. S. Babu, S. Jana, and M. Lindner, J. High Energy Phys. 10 (2020) 040.
[43] S.-L. Chen, A. Dutta Banik, and Z.-K. Liu, Nucl. Phys. **B966**, 115394 (2021).
[44] R. A. Lineros and M. Pierre, J. High Energy Phys. 21 (2020) 072.
[45] I. M. Ávila, V. De Romeri, L. Duarte, and J. W. F. Valle, Eur. Phys. J. C **80**, 908 (2020).
[46] L. Lopez Honorez, E. Nezri, J. F. Oliver, and M. H. G. Tytgat, J. Cosmol. Astropart. Phys. 02 (2007) 028.
[47] R. Barbieri, L. J. Hall, and V. S. Rychkov, Phys. Rev. D **74**, 015007 (2006).
[48] E. M. Dolle and S. Su, Phys. Rev. D **80**, 055012 (2009).
[49] J. R. Ellis, A. Ferstl, and K. A. Olive, Phys. Lett. B **481**, 304 (2000).
[50] A. V. Semenov, arXiv:hep-ph/9608488.
[51] A. Pukhov, E. Boos, M. Dubinin, V. Edneral, V. Ilyin, D. Kovalenko, A. Kryukov, V. Savrin, S. Shichanin, and A. Semenov, arXiv:hep-ph/9908288.
[52] G. Belanger, F. Boudjema, A. Pukhov, and A. Semenov, Comput. Phys. Commun. **176**, 367 (2007).
[53] G. Belanger, F. Boudjema, A. Pukhov, and A. Semenov, Comput. Phys. Commun. **180**, 747 (2009).
[54] N. Aghanim *et al.* (Planck Collaboration), Astron. Astrophys. **641**, A6 (2020).
[55] J. Aalbers *et al.* (LZ Collaboration), Phys. Rev. Lett. **131**, 041002 (2023).
[56] S. Kashiwase and D. Suematsu, Eur. Phys. J. C **73**, 2484 (2013).
[57] S.-Y. Ho and J. Tandean, Phys. Rev. D **87**, 095015 (2013).
[58] S. Singirala, Chin. Phys. C **41**, 043102 (2017).
[59] I. Esteban, M. C. Gonzalez-Garcia, M. Maltoni, T. Schwetz, and A. Zhou, J. High Energy Phys. 09 (2020) 178.
[60] S. Roy Choudhury and S. Choubey, J. Cosmol. Astropart. Phys. 09 (2018) 017.
[61] C. Giunti, K. A. Kouzakov, Y.-F. Li, A. V. Lokhov, A. I. Studenikin, and S. Zhou, Ann. Phys. (Amsterdam) **528**, 198 (2016).
[62] E. Aprile *et al.* (XENON Collaboration), Eur. Phys. J. C **80**, 785 (2020).
[63] J. N. Bahcall and C. Pena-Garay, New J. Phys. **6**, 63 (2004).
[64] I. Lopes and S. Turck-Chièze, Astrophys. J. **765**, 14 (2013).
[65] P. A. Zyla *et al.* (Particle Data Group), Prog. Theor. Exp. Phys. **2020**, 083C01 (2020).